



Framework to predict the orientation of fibers in FRC: A novel philosophy

F. Laranjeira ^{a,*}, A. Aguado ^a, C. Molins ^a, S. Grünewald ^b, J. Walraven ^b, S. Cavalaro ^a

^a Department of Construction Engineering, Universitat Politècnica de Catalunya, Barcelona, Spain

^b Section of Concrete Structures, Delft University of Technology, The Netherlands

ARTICLE INFO

Article history:

Received 9 March 2011

Accepted 21 February 2012

Keywords:

Fiber reinforcement (E)

Vibration (A)

Fresh concrete (A)

Tensile Properties (C)

Modeling (E)

ABSTRACT

This paper aims at providing a link between fiber orientation and the properties of FRC, the structure to be built and its respective production process. Since the proposed framework is to a large extent new, the main components are described in the beginning. Then, two major subjects are approached from a theoretical perspective: fiber orientation in 3-D and the wall-effects of fibers in anisotropic conditions. Finally, in the last part, the main steps of the proposed framework are analyzed in detail and validated with experimental results. This comprehensive and straightforward model has shown to be capable of estimating the average orientation of fibers with very good accuracy. Thereby, this paper is a meaningful contribution to create an engineering toolbox for the prediction of fiber orientation in practical applications of fiber reinforced concrete.

© 2012 Elsevier Ltd. All rights reserved.

1. Introduction

Adding fibers to cement-based materials has been widely studied in the last decades. Since then, the advantages of using fiber reinforced concretes (FRC) became evident and gradually attracted the interest from the construction industry. Consequently, the use of this material increased both in quantity and diversity, with innumerable examples of applications being reported in literature [1–3]. In the present, the industry is demanding to apply FRC for structural purposes, which has already been shown to be a feasible solution through some successful applications worldwide [1–4]. However, although the future of FRC is promising from a technical perspective, its generalized application requires a tailored material in order to become economically competitive against traditional solutions. In this context, a cost-contained way to optimize FRC is the application of specific production processes that generate preferential fiber orientations at the locations and directions of the structural element submitted to higher stresses. In other words, fiber orientation should be predictable so that FRC could satisfy both technical and economical restraints more effectively. A framework embracing the major influencing mechanisms of fiber orientation in a rational and design-oriented approach is therefore of paramount importance.

Among the several aspects governing fiber orientation, the wall-effects introduced by the sides of the mold [5–13] and the fresh-

state properties of FRC [14–18] are most affecting. The way concrete is poured into the mold has also been recognized to have a major impact on fiber orientation, both due to the casting direction and due to preferential fiber alignment induced by the casting element itself [19–21]. The effects of vibration on causing fibers to rotate into planar orientations have been reported in literature [22,23] and, in case of self-consolidating concrete (SCC), the flow of the fresh concrete has also been identified to play a major role on fiber alignment [14,16,24].

Research on fiber orientation has been carried out mostly from an experimental perspective and the few advanced theoretical approaches refer uniquely to the quantification of wall-effects on idealized isotropic FRC [13]. How to quantify the combined influence of all the aforementioned aspects on fiber orientation is therefore a big question mark.

The average fiber orientation in a certain direction is generally considered through the so-called orientation number (η). This parameter is frequently applied on experimental investigations to quantify the influence of one of the aforementioned aspects on fiber orientation by isolating it from the others. For instance, the effect of the casting direction has been quantified by considering elements poured in different positions while keeping all the remaining aspects constant [19,21]. Another example consists on inferring the effects of compaction by subtracting from the measured η the theoretical values of idealized isotropic FRC affected by the wall-effects [8].

Both procedures are straightforward and allow gaining insight on the magnitude of the influence that each aspect has on fiber alignment. Hence, up to the present, the parameters governing fiber orientation are approached independently from each other, i.e., from an isolated perspective (Fig. 1). However, considering the nature of these aspects, its determination through such isolated perspective is arguable.

* Corresponding author. Tel.: +34 934017347; +34 934054135.

E-mail addresses: filipe.laranjeira@upc.edu (F. Laranjeira), antonio.aguado@upc.edu (A. Aguado), climent.molins@upc.edu (C. Molins), s.grunewald@tudelft.nl (S. Grünewald), j.c.walraven@tudelft.nl (J. Walraven), sergio.pialarissi@upc.edu (S. Cavalaro).

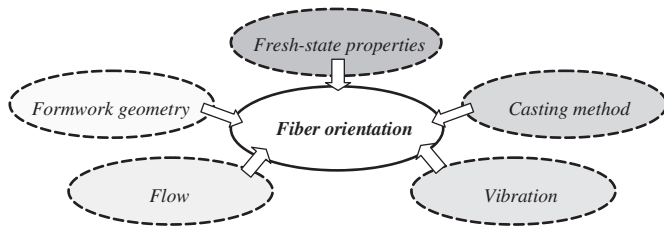


Fig. 1. Scheme of the current approach to evaluate fiber orientation: an isolated perspective.

Can preferential fiber alignment induced by the casting direction be quantified by disregarding the type of casting element applied?

Is it reasonable to account for the wall-effects of the mold under an isotropic fiber orientation assumption when anisotropy due to fresh-state properties, casting and compaction processes is likely to occur?

The answer to these questions seems to be obvious. By making use of an isolated procedure, fiber orientation can only be quantified for the very specific characteristics of materials and production processes applied and for the geometry of the element produced. Conclusions extracted with such a procedure are therefore limited and it is hardly possible to extrapolate for different scenarios.

In this paper, the orientation of fibers is analyzed and predicted through a novel philosophy because the properties of FRC, the structure to be built and its respective production process are included through logical and well-structured concepts. Firstly, the outline of the new framework is presented and its core concepts are highlighted. Then, the fiber orientation is evaluated in the spatial domain, both with a theoretical- and a probabilistic and experimental approach, which provides better insight compared to 1-D analysis commonly covered in literature. Subsequently, the wall-effects are studied in detail and a theoretical approach is advanced for its quantification both in isotropic and anisotropic conditions.

The framework proposed in this paper attempts to evaluate fiber orientation from a wider perspective than mere particular cases, including theoretical concepts to explain some of its major aspects and bringing together the combined influence of material properties, production processes and the structure itself. The goal of this paper is not to present a final operational framework, but rather serves, hopefully, to provide a step towards the development of a rational and design-oriented procedure. If fiber orientation could be predicted this way, comprehensive and cost-effective designs of FRC applications could be performed [25].

2. Framework outline

Fiber orientation in the hardened-state is the final result of a chain of stages that FRC passes through from mixing to hardening inside the formwork. The specific boundary conditions that characterize each phase of the production process induce many stages of interaction at which fiber orientation is modified.

The transient fiber orientation at the end of each of these stages depends on the specific type of action imposed (wall-effects, gravity, external vibration, etc.), but also on the predominant orientation existing prior to each stage. Hence, the several aspects governing fiber orientation cannot be evaluated independently but rather shall be approached from an integrated and sequential perspective of the overall production process through a step-by-step procedure. For that purpose, four transient orientation numbers prior to the final one in the hardened-state (η_0) are defined in order to provide a logical approximation:

- concrete fresh-state properties after mixing (η_M)
- after casting into the formwork (η_C)

- after occurrence of dynamic effects (such as vibration or flow) (η_D)
- after the wall-effects introduced by the formwork (η_F) (Fig. 2).

In order to quantify and to establish the interdependence of the several orientation numbers occurring along the production process, two major topics need to be covered: 1) fiber orientation in the spatial domain; and 2) wall-effects in anisotropic conditions. Both subjects are discussed in the following sections as a first attempt to predict fiber orientation through this new framework.

3. Fiber orientation from a 3-D perspective

Although FRC has been extending its field of applications, this material probably performs best when 2-D or 3-D stresses are concerned. Because fibers are everywhere and oriented in all directions they can cope with any expected and unexpected stresses, wherever in concrete [26]. Mechanical properties and fiber orientation of FRC shall therefore be evaluated globally, regarding not only one but several different directions.

When measuring η , the fiber orientation is evaluated along one unique axis. Its value varies from 0.0 to 1.0, referring to fibers orthogonal and parallel to the analyzed direction, respectively. If a fiber rotating in space is now considered, when preferential orientation is observed along a certain axis, the projected fiber lengths on the remaining two independent axes decrease. The orientation numbers in three independent axes are therefore evidently correlated. How they depend on each other and what are their theoretical and probabilistic ranges of variation is presented herein and compared to experimental results.

3.1. Theoretical and probabilistic envelop curves

The relationship between the orientation numbers in three independent axes can be analyzed by calculating the spherical coordinates of all the possible positions of fiber end-points. Fixing fiber length (L) as a unitary vector, η in x-, y- and z-directions become uniquely defined through horizontal and vertical angles (β and φ , respectively), such as shown in Fig. 3.

For practical purposes, more than determining the theoretical range of variation of η in the spatial domain, a probabilistic confidence interval is demanded. Thereby, the probability of occurrence of the governing angles (β and φ) has to be related with each of the orientation numbers.

Under isotropic conditions, any point of the spherical surface shown in Fig. 3 has an equal probability of occurrence. However, the chances that a fiber is nearly aligned with any of the independent axes are quite small. To support this statement consider Fig. 4, in which a small angle ξ around each of the independent axes is related with its respective probability of occurrence (A_ξ) in half of the sphere.

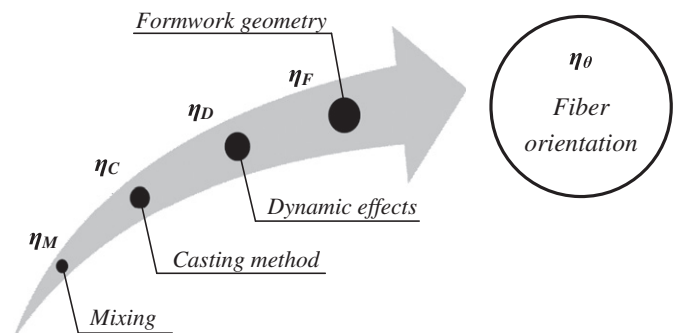


Fig. 2. Main stages of the production process and respective orientation numbers.

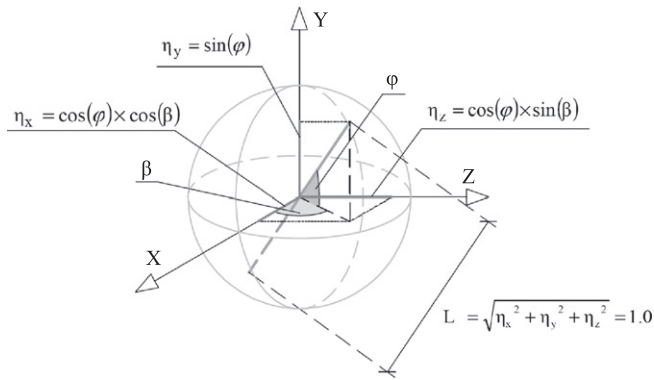


Fig. 3. Characterization of fiber orientation through two independent angles.

The latter corresponds to the surface of a sphere cap which is defined by:

$$A_{\xi} = \frac{\pi \times L^2}{2} \times (1 - \cos \xi) \quad (1)$$

Regarding that six sphere caps can be extracted from a sphere, it is possible to define a certain significance level (SL) up to which the probability of occurrence is depreciable:

$$SL = \frac{6 \times A_{\xi}}{A_{\text{sphere}}} = 3 \times (1 - \cos \xi_{SL}). \quad (2)$$

By selecting a significance level of 0.10, the respective angle around each of the axis (ξ_{SL}) returns a value of about 15°. Consequently, the 90% confidence intervals for β and φ (in degrees) can be derived:

$$\varphi_{(SL=0.10)} \in [0, 75] \quad (3)$$

$$\beta_{(SL=0.10)} \in \begin{cases} [0, 90] & \text{if } \varphi \geq 15^\circ \\ [0, 90 - 2 \times (15 - \varphi)] & \text{if } \varphi < 15^\circ \end{cases} \quad (4)$$

To identify the correlation between η in 3-D a parametric study was carried out by varying both β and φ along their entire ranges of variation. Then the fiber projected lengths were obtained, as shown in Fig. 3, and the sums of the orientation numbers in the horizontal plane (η_{xz}) and in the spatial domain (η_{xyz}) were calculated, according to Eqs. (5) and (6). The dependency of η_{xz} and η_{xyz} with β and φ are presented in Fig. 5, both for their theoretical and probabilistic ranges of variation.

$$\eta_{xz} = \eta_x + \eta_z \leq \sqrt{2} \quad (5)$$

$$\eta_{xyz} = \eta_x + \eta_y + \eta_z \leq \sqrt{3}. \quad (6)$$

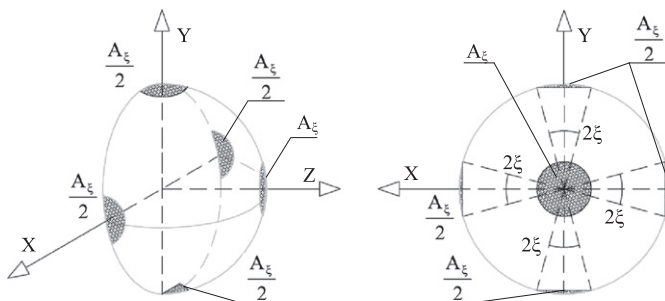


Fig. 4. Identification of the significance level of half of the spherical surface.

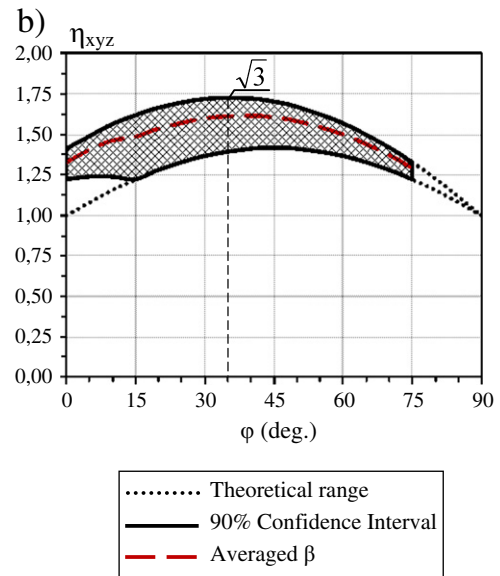
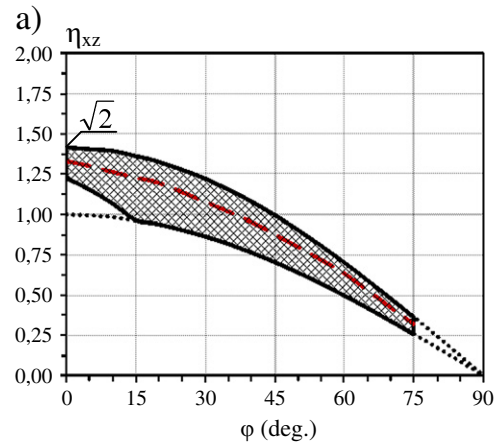


Fig. 5. Theoretical and probabilistic ranges of variation of: a) 2-D and b) 3-D.

Fig. 5a shows the influence of the vertical angle (φ) on the horizontal plane for any value of β. When increasing φ, both the magnitude and the amplitude of the theoretical η_{xz} decrease progressively towards a zero value. On the other side, when accounting for the aforementioned 90% confidence interval, minimum and maximum values of 0.26 and 0.37 can be found when φ equals 75°. For vertical angles smaller than 15°, the reduced amplitude of variation of η_{xz} due to the restrained range of β is noticeable.

By analyzing the variation of the orientation numbers in the spatial domain (Fig. 5b) it can be observed that, although the amplitude of the theoretical η_{xyz} decreases with φ, its magnitude no longer varies monotonically. A maximum value can be observed ($\sqrt{3}$) when β is equal to 45° and φ approaches 35°. The probabilistic confidence interval applies such as in the previous case, defining a minimum value for η_{xyz} of about 1.23 that is verified when φ is equal to 0°, 15° and 75°. The upper bound of both η_{xz} and η_{xyz} occurs when β is equal to 45° whereas the lower bound refers to fibers whose projection in the horizontal plane coincides with the main axes x and z (β equal to 0° and 90°).

Results shown in Fig. 5 are relevant as they fix the theoretical and most probable range of variation for the sum of orientation numbers in different directions through a correlation with the horizontal and vertical angles. This way, changes on preferential fiber alignments such as the ones imposed by the direction of casting can be intuitively explained.

3.2. Experimental verification

The theoretical and probabilistic envelop curves presented in Section 3.1 are general and apply for any situation. In order to validate them, the experimental work performed by Molins et al. [27] was taken into account as an example. In the latter, four cylindrical samples with 100 mm diameter and 150 mm height were extracted in different directions from a bending test specimen and the fiber orientation was analyzed through the computerized tomography technique (CT-scans). In all the samples, axial tomographies of the cross-sections were taken with a constant spacing of 1 mm along the height, thus providing the exact number and orientation of fibers in 3-D. The applied FRC was a SCC with 20 kg/m³ steel fibers (60 mm length; 0.75 mm diameter).

The results obtained by [27] identified a total of 686 fibers, 118 of which were completely embedded in the analyzed samples. The orientation numbers of all the single fibers were calculated for the three independent axes and the results of η_{2D} and η_{3D} are compared with the theoretical and probabilistic envelop curves in Figs. 6 and 7, respectively, where triangles refer to each of the 686 fibers from [27].

The experimental average of the sum of orientation numbers in 2-D ($\eta_{kz,m}$) was approximately 1.15 with a standard deviation, $\sigma(\eta_{kz})$ of 0.19. On the other hand, the respective average of the sum of orientation numbers in 3-D ($\eta_{kxyz,m}$) was 1.48 with a standard deviation ($\sigma(\eta_{kxyz})$) of 0.16. According to the investigation performed by Laranjeira et al. [25] the Gaussian law is capable to describe the statistical distribution of fiber orientation. According to the properties of such law, the intervals $[\eta_{kz,m} - 2\sigma(\eta_{kz}), \eta_{kz,m} + 2\sigma(\eta_{kz})]$ and $[\eta_{kxyz,m} - 2\sigma(\eta_{kxyz}), \eta_{kxyz,m} + 2\sigma(\eta_{kxyz})]$ should contain at least 95.4% of the fibers. Indeed, 97.4% and 95.3% of the fibers were observed within these limits in Figs. 6a and 7a, respectively.

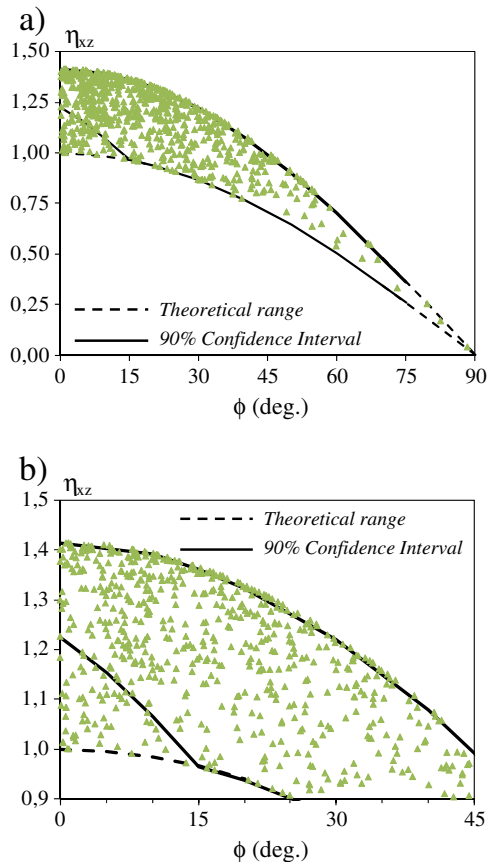


Fig. 6. Experimental verification of η_{kz} : a) overall results; and b) detailed analysis.

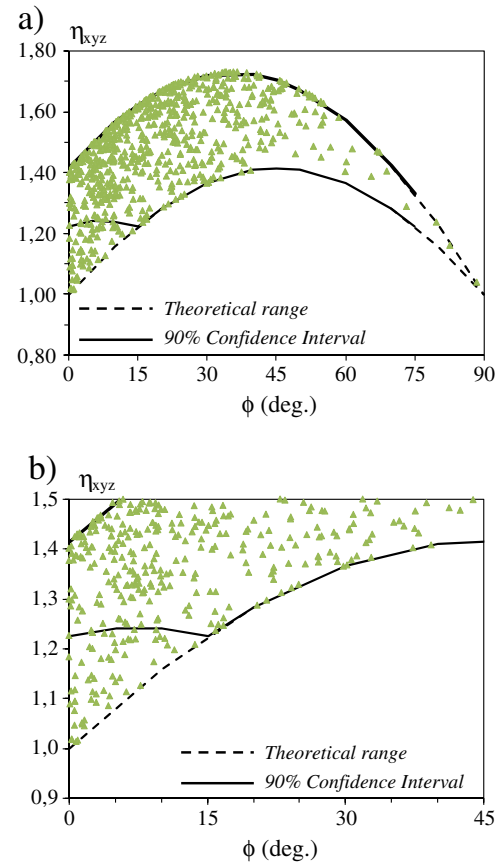


Fig. 7. Experimental verification of η_{kyz} : a) overall results; and b) detailed analysis.

A second conclusion derived from Figs. 6 and 7 is that η_{kz} and η_{kxyz} are always within the theoretical enveloping curves presented. Furthermore, also the suitability of the probabilistic approach could be verified, with η_{kz} and η_{kxyz} providing values that support the predefined confidence interval (91.5% and 91.3%, respectively).

4. Approach to estimate generalized wall-effects

The calculation of the orientation number has been of interest of many researchers [5–13]. Analytical formulations proved that η in isotropic conditions for 1-D, 2-D and 3-D are equal to 1.0, $2/\pi$ and 0.5. However, despite the interest of these values, their applicability is very limited since the restraining action introduced by external boundaries on fiber rotation is not considered.

It should be mentioned that the magnitude of the wall-effects depends on the type of fibers. In this framework, these effects are accounted for fibers with high stiffness (i.e. steel). An additional parameter would be necessary in order to convert these effects for other types of fibers.

In order to take into account the influence of wall-effects on the orientation number, Dupont and Vandewalle [13] advanced an averaging procedure by identifying the zones of the cross-section with none, one and two boundary conditions (A_0 , A_1 and A_2) and then attributing their respective average orientation numbers (η_0 , η_1 and η_2), as shown in Fig. 8. The authors assumed the extent of the influence zone based on the assumption that fibers rotate over their center of gravity. They also assumed that the center of gravity defines the location of a fiber and that such point has an equal probability of occurrence within the cross-section. They considered that the top surface of the section has the same boundary condition (BC) as the sides of the mold and that no differences exist between straight and hooked-end fibers concerning the calculation of η . Through the

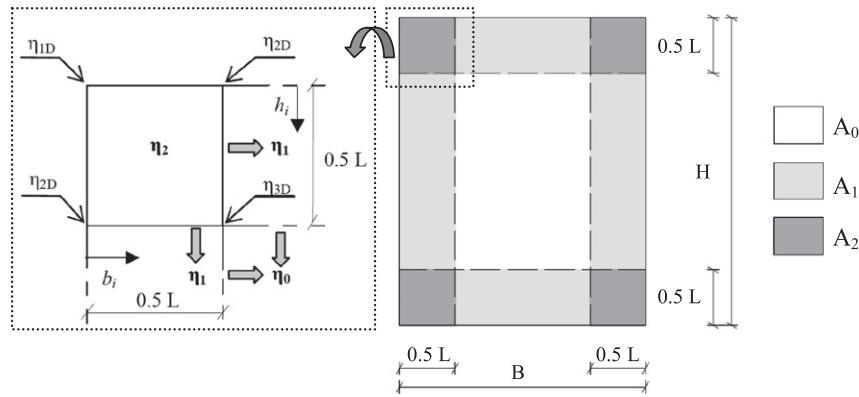


Fig. 8. A cross-section divided in three zones (with detail of the corner).

development of a mathematical model, the average orientation numbers under the influence of one BC (η_1) and two BCs (η_2) were found to be approximately equal to 0.60 and 0.84, respectively.

Despite the relevant work reported by [13], a major limitation is the fact that the procedure is only applicable under the assumption of isotropic conditions, i.e., that the orientation number in the bulk (η_0) coincides with the one in the spatial-random case, η_{3D} (0.50). However, the reasonability of this hypothesis is highly arguable regarding that preferential fiber orientation is likely to occur due to several aspects (casting procedures, vibration, flow, etc.). Consequently, the actual influence of wall-effects on η will differ: if fibers in bulk are mostly orthogonal to one BC, the increment of fiber alignment in the direction parallel to that BC will be much larger than in the case that fiber in bulk would have already some preferential orientation parallel to the BC. Thereby, η_1 and η_2 shall be adapted consistently to any orientation number in bulk (η_0) in order to obtain generalized wall-effects.

4.1. Analysis of the wall-effects in isotropic conditions

The numbers η_1 and η_2 result from an averaging process which simplifies a much more complex behavior. In fact, a realistic distribution of the orientation number nearby a wall(s) consists of a progressive transition zone that bridges η_0 to the one close to the wall(s) (2-D or 1-D cases). In order to determine the nature of such transition relationships, η has to be calculated systematically by considering the fiber gravity point at different distances from the wall(s). By using the formulations advanced in the aforementioned work [13], heavy and slowly convergent numerical integrations have to be carried out. A more simple and analytical alternative approach is proposed in Appendix 2.

By applying the expressions included in Appendix 2, η can be easily calculated for different distances between fiber gravity point and

both walls, such as presented in Fig. 9. The average orientation number obtained along the influence zone of one BC for the spatial-random case (η_1) supports the value advanced in [13]: 0.60. In the planar-random case ($h_i/L=0$) an average orientation number of 0.93 was obtained. The average of all curves along h_i provides an average orientation number at the corner of the section of about 0.84, thus confirming the value previously advanced [13].

4.2. Approaching the wall-effects in anisotropic conditions

At a first glimpse, the results provided in Fig. 9 may seem excessively minutia and with none practical application. However, valuable information on fiber orientation can be extracted from it. First of all, the average of the diagrams shown in Fig. 9 support the values advanced in literature [13] for fibers in isotropic conditions under the influence of one and two BCs. Thereby, adjusted η_1 and η_2 can be easily obtained for any cross-section in isotropic conditions when the shorter dimension is smaller than the fiber length.

A nonlinear transition can be observed in Fig. 9, with η barely decreasing at short distances from the wall and then denoting a less pronounced wall-effect when the fibers' gravity point approaches a distance equal to half the fiber length. Given these consistent results, a simplified bilinear diagram is hereafter proposed to approach such behavior (Fig. 10). In the case of one BC, the fiber orientation reflects the transition between η_{2D} at the wall (≈ 0.637) and η_{3D} in bulk (≈ 0.50), providing an average value (η_1) of 0.60. Considering these values, the equivalent bilinear diagram becomes defined by fixing the intermediate point of the diagram at a distance of about 0.23 times the fiber length (Fig. 10).

When two orthogonal BCs exist, the influence of one wall on η depends on the distance of the fibers' gravity point relative to the other orthogonal wall, thus different transition diagrams (Fig. 9) are obtained, which provide an average η_2 equal to 0.84. This value can

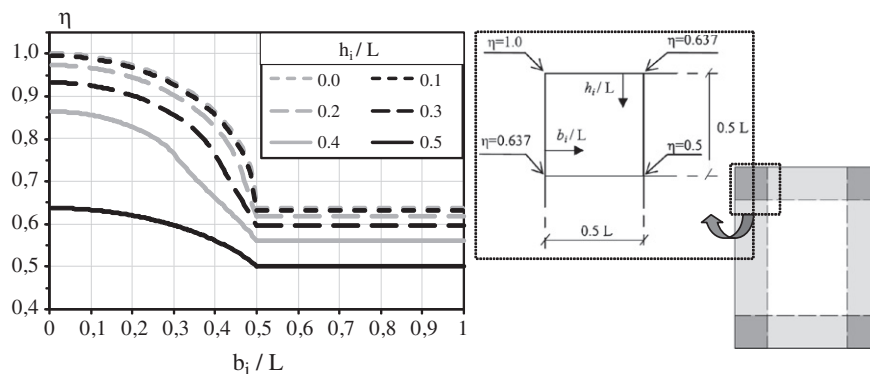


Fig. 9. Variation of η at different distances from both walls.

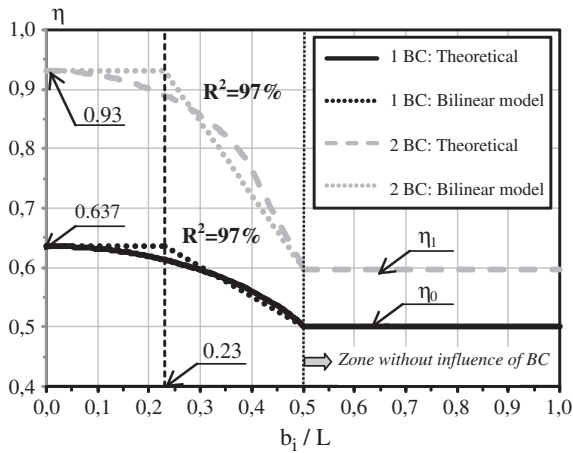


Fig. 10. Bilinear models to approach wall-effects under isotropic conditions.

be interpreted as the average η between the extreme cases (b_i/L equal to 0.0 and 0.50), whose representative averages of η are 0.93 and 0.60, respectively. Thereby, when calculating the bilinear diagram with these extreme values and an average of 0.84, the intermediate point of the diagram turns out to be, again, at a distance of about 0.23 times the fiber length from the wall (Fig. 10). Such feature of the bilinear diagrams provide ground to justify from a theoretical perspective that, up to a distance of about 0.23 times the fiber length, the fiber orientation is higher than in the remaining zone under the influence of the wall. This conclusion is supported by experimental observations [9], which found different densities of fibers within the band of influence of the wall, particularly larger values on the region closest to the mold surface.

Given the existence of a bandwidth close to the walls with approximately constant orientation numbers (0.93 and 0.637) and the fact that η at distances from the walls equal to half the fiber length are always equal to η_0 , the bilinear diagrams shown in Fig. 10 provide a tool to define the wall-effects for any anisotropic scenario. This way, η_1 and η_2 can be generalized as a function of the orientation number in bulk (η_0), such as defined by Eqs. (7) and (8). These expressions are valid whenever fiber alignment is affected by the walls (η_1 and η_2 equal or greater than η_0). In cases with fibers having large orientation numbers in bulk (large η_0), Eqs. (7) and (8) may not be verified. This is typically the case with fibers which are already oriented parallel to the walls that the latter does not have any influence. In those cases, η_1 and η_2 shall be assumed equal to η_0 .

$$\eta_1 = 0.465 + 0.270 \cdot \eta_0 \quad (\geq \eta_0) \quad (7)$$

$$\eta_2 = 0.677 + 0.270 \cdot \eta_1 \quad (\geq \eta_0). \quad (8)$$

By applying Eqs. (7) and (8) in the averaging procedure depicted in Fig. 8, the wall-effects can then be quantified for any anisotropic conditions ($\eta_0 \neq 0.50$). The increments of orientation number due to the wall-effects ($\Delta\eta_w$) are quantified in Appendix 3 for common cross-section geometries (rectangular, circular and hollow-circular).

5. Framework analysis: step-by-step

Taking into account the theoretical concepts advanced in Sections 3 and 4, some of the major aspects governing fiber orientation become clear and physically explained.

In this part of the paper, the main stages of the production process influencing fiber orientation (Fig. 2) are discussed:

1. Mixing (η_M)
2. Casting method (η_C)

3. Dynamic effects (η_D)
4. Formwork geometry (η_F)

Firstly, relevant experimental evidence and conclusions reported in literature are highlighted. Then, based both on theoretical and experimental results, a first attempt is advanced to quantify each of the four transient orientation numbers. A step-by-step methodology was adopted in order to integrate several production stages within a rational procedure. A brief summary of the main steps of the framework is shown at the end of this section.

5.1. Influence of fresh-state properties after mixing

One of the major aspects governing fiber orientation is the rheology of FRC. Although the latter has been subject of extensive research, standardized equipment and measuring techniques are not yet available and therefore its correlation with the orientation of fibers in fresh concrete is unknown [28]. Hence, given the scarce knowledge about this subject, fiber orientation will be herein approached by simply distinguishing the behavior of conventional and self-compacting FRC in the fresh-state. Conventional concrete (CC) is a granular mass requiring vibration to be compacted while self-compacting concrete (SCC) is a liquid suspension following the rules of fluid mechanics [29]. Thereby, fiber orientation in the three independent axes after mixing is likely to be different according to the type of concrete considered.

CC mixtures are homogeneous due to lack of flow-ability and therefore the orientation of fibers may be random in three dimensions when the material is discharged from the mixer [22]. According to the theoretical range of variation of η_{xyz} in isotropic conditions (Fig. 5b), an average constant value within the predefined confidence interval can be obtained by averaging the two independent angles β and φ . In such conditions, η_{xyz} is equal to 1.50 with a small coefficient of variation (CV) of 7.9%. Because isotropy conditions imply the absence of preferential fiber alignment, η_M of CC can then be assumed to be equal to 0.50 in three independent axes.

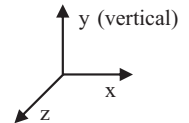
In contrast, a mixture with increased flow-ability in the fresh-state shows a stronger alignment of the fibers than a material with lower flow-ability [30]. SCC requires filling ability for horizontal and vertical flow, thus being prone to induce planar orientation of fibers. The flow can be idealized as taking place in layers that force fibers which are crossing them to align along their borderlines [14]. The latter can then be idealized as virtual boundaries which restrain the rotation capacity of fibers. In this approach, the thickness of these virtual layers is assumed to be equal to the fiber length (L), which according to the expressions of the wall-effects for isotropic conditions, returns an average η of 0.60 in the two independent directions of the horizontal plane (η_{Mx} and η_{Mz}). Consequently, according to the average value of 1.50 advanced for η_{xyz} in 3-D, η along the remaining direction (η_{My}) would be equal to 0.30. The orientation numbers after mixing of FRC considered (η_M) are summarized in Table 1:

5.2. Influence of the casting method

Several researchers have reported remarkable influences of casting elements [19–21], casting direction [21,30,31] and casting height [35]

Table 1
Summary of considered η_M according to direction and type of concrete.

Type of concrete	η_{Mx}	η_{My}	η_{Mz}
CC: conventional	0.50	0.50	0.50
SCC: self-compacting	0.60	0.30	0.60



on fiber orientation. Consequently, in order to be able to compare properties of different FRCs, casting methods have to be exactly the same (described and reproducible) [30]. These facts lead to the obvious conclusion that the non-uniformity of fiber orientation due to different casting methods has to be considered in the design of structural elements [24]. This explains tremendous differences in structural performances sometimes observed in elements with the same FRC poured in different directions. However, its influence cannot be evaluated independently from other aspects. Indeed, the casting direction was found to have a paramount influence on the mechanical properties of fluid fibrous mixtures, but a significantly smaller effect was observed with more viscous mixtures [19]. The link between the casting method and the rheological properties of fresh concrete is of utmost importance [32].

The effect of the casting height on fiber orientation at the point where concrete is poured into the formwork may have some influence on fiber orientation, particularly on concretes with larger flow abilities. In fact, the flow movement at the zone where concrete contacts the formwork or already poured concrete may generate significant disturbances on fiber orientation. The degree to which this aspect is important depends on the rheological properties of concrete and on the shape of the element. At decreasing yield value the concrete tends to distribute quicker from the point of casting, which increases the ratio of affected zone compared to the cast height of concrete at this point [35]. Therefore, at increasing casting heights and concrete flow abilities, increasing reductions on the orientation number aligned with the gravity axis would be expected. Because the proposed framework focuses on the estimation of fiber orientation on current cross-sections, such zone of disturbance was assumed to have a very limited extension and, consequently, no parameter accounting for this local phenomenon was considered. If the flow ability is high and the extension of the element relatively large compared to the casting point, a parameter accounting for the casting height (C_{Hi}) should be added to Eq. (10).

The effect of pouring elements on fiber orientation may be somehow irrespective of the type of element applied (e.g.: skip, trolley, shovel, bucket, etc.), but rather mainly dependent on the geometry of their exit cross-sections. Therefore, the generalized expressions presented in Appendix 3[25] can be used to quantify the increment of orientation number due to wall-effects introduced by the casting element ($\Delta\eta_{CW}$). The orientation number in bulk of the casting element (η_{CO}) should account for the casting direction (previously defined in terms of φ and β in Fig. 4) and for the fresh-state properties of the concrete after mixing (η_M), according to Eq. (9):

$$\eta_{CO} = \sqrt{(\eta_{Mx} \times \cos\varphi \times \cos\beta)^2 + (\eta_{My} \times \sin\varphi)^2 + (\eta_{Mz} \times \cos\varphi \times \sin\beta)^2}. \quad (9)$$

Then, η have to account for the wall-effects through a parameter referring to the misalignment between the casting element and the main axes of the formwork in direction i (C_{Di}). For that purpose, the same referential adopted for concrete properties (Fig. 3) will be considered. In such hypothesis, the increment of η due to casting method within any direction i ($\Delta\eta_{Ci}$) can be obtained (Eq. (10)). Consequently, η after casting FRC into the formwork along any direction i (η_{Ci}) is given by Eq. (11).

$$\Delta\eta_{Ci} = \Delta\eta_{CW} \times C_{Di} \quad (10)$$

$$\eta_{Ci} = \eta_{Mi} + \Delta\eta_{Ci}. \quad (11)$$

According to the analysis in the 3-D domain advanced in Section 3, η in the three main axes depends on the two governing angles φ and β . The introduction of a preferential orientation due to the wall-effects changes the representative angles φ and β of all fibers in the section and, consequently, η in the two remaining axes are also modified. This phenomenon will be herein defined as secondary wall-effects. The latter cannot be quantified arbitrarily, but rather have to be consistent with the nature

of the BCs that generated the wall-effects. Consider, for instance, the case where the casting method accounts for a pouring element with rectangular exit cross-section and aligned along the x-axis of the formwork (Fig. 11). Since the geometry of the cross-section implies different effects of vertical and horizontal boundaries ($B_C > H_C$) it seems reasonable to apply a criterion proportional to their respective perimeter fractions (Eqs. (12)–(14)). This way, the higher the perimeter fraction of one border of the casting element, the larger will be the reduction of η in the direction orthogonal to such border. Note that η_{xyz} is kept constant regarding that, as previously shown, it provides a reasonable approximation within the defined probabilistic confidence interval.

$$\Delta\eta_{Cx} = \Delta\eta_{CW} \quad (12)$$

$$\Delta\eta_{Cy} = -\Delta\eta_{CW} \times \frac{B_C}{B_C + H_C} \quad (13)$$

$$\Delta\eta_{Cz} = -\Delta\eta_{CW} \times \frac{H_C}{B_C + H_C}. \quad (14)$$

Regarding the previous example, general expressions to quantify the parameters accounting for the misalignment between casting element and the formwork in the three main axes (C_{Dx} , C_{Dy} and C_{Dz}) can be advanced (Table 2). For circular geometries, B_C and H_C may be chosen equal to the diameter of the cross-section.

In the case of self-compacting FRC, the high flow ability of the material tends to decrease the orientation number of fibers in the y-axis. Thereby, once FRC is cast inside the formwork, the effects introduced by BCs orthogonal to the y-axis may be depreciable since the material will tend to denote a preferential planar-orientation. For SCC, η_{Cy} should remain equal to η_{My} . Consequently, a fictitious BC orthogonal to the gravity axis may be assumed, implying that H_C equals L . If the casting is performed with free top surface, H_C is the minimum value between L and two times the geometric H_C of the casting element.

5.3. Influence of dynamic effects

After casting FRC the orientation of fibers may be modified due to dynamic effects that take place in order to guarantee appropriate filling of the formwork. In the origin of these dynamic effects, the external vibration process applied on conventional FRC and the flow of self-compacting mixtures are paramount stages. Thereby, η after the occurrence of dynamic effects in direction i (η_{Di}) depends on the pre-orientation of fibers once cast into the formwork (Eq. (15)) and shall account for the respective variations due to external vibration and flow, $\Delta\eta_{DVi}$ and $\Delta\eta_{DFi}$, respectively (Eq. (16)).

$$\eta_{Di} = \eta_{Ci} + \Delta\eta_{Di} \quad (15)$$

$$\Delta\eta_{Di} = \Delta\eta_{DVi} + \Delta\eta_{DFi}. \quad (16)$$

5.3.1. The effect of external vibration

Vibration may cause rotation and alignment of the fibers preferentially in a specific direction [23]. External vibration tends to orient

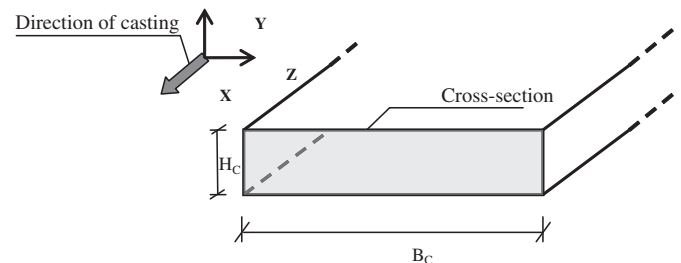


Fig. 11. Example of cross-section of a casting element aligned with the x-axis.

Table 2Summary of C_{Di} in the three main axes of the formwork.

$$\begin{aligned}
 C_{Dx} &= \cos\varphi \times \cos\beta - \sin\beta \times \frac{H_{C,eff} \times \cos\varphi}{B_C + H_{C,eff}} \\
 C_{Dy} &= \sin\varphi - \cos\varphi \times \frac{B_C}{B_C + H_{C,eff}} \\
 C_{Dz} &= \cos\varphi \times \sin\beta - \cos\beta \times \frac{H_{C,eff} \times \cos\varphi}{B_C + H_C}
 \end{aligned}$$

fibers in a plane perpendicular to the direction of vibration [22], with the tendency towards a planar fiber orientation [8,11,23]. Robbins et al. [33] reported that there is essentially no difference between poured FRC subjected to external vibration and sprayed concrete in terms of fiber distribution and orientation [33]. Vibration does not have a significant effect on fiber orientation if the specimen is only vibrated for 1 or 2 min and if the workability of the concrete is not too high, whereas excessive vibration leads to preferential orientation of fibers together with segregation [23].

According to experimental evidence, external vibration has a direct influence on fiber orientation along the gravity axis (η_y): the more FRC is vibrated, the more fibers tend to align in the horizontal plane, thus decreasing η_y . According to the probabilistic analysis advanced in Section 3, the latter will likely vary between 0.30 and 0.95. Although the qualitative effect of external vibration is indisputable, its quantification remains unknown. Consequently, it is required to investigate the influence of the energy, frequency and duration of vibration on fiber orientation of mixtures with different properties in the fresh-state and various fiber types. If the decrease in the y-axis could be quantified ($\Delta\eta_{Dvy}$), $\Delta\eta_{Dvx}$ and $\Delta\eta_{Dvz}$ would compensate it in the same way, providing that constant η_{xyz} holds a reasonable assumption.

5.3.2. The effect of the flow

Fresh cementitious materials behave as fluids with a yield stress (τ_{00}), which is the minimum stress for irreversible deformation and flow to occur. This parameter controls whether or not concrete will start or stop flowing under an applied stress, thus being the most important property for the filling ability of SCC [32]. However, due to the thixotropic behavior of cementitious materials, there is an evolution of the rheological properties from the end of the mixing phase until casting and hardening occurs. In thixotropic materials, flocculation and de-flocculation occur at rest and under flow, respectively. For fresh plain concrete the first one is far more important regarding that, on the aspects of major practical interest (formwork pressure and multi-layer casting), concrete is indeed not flowing [32]. Nonetheless, in the case of fresh FRC, fiber orientation tends to be the major concern and thereby the process of de-flocculation may also play an important role.

When FRC flows along the formwork a certain flow profile develops, most likely due to frictional restraint with the walls of the formwork [30], and fibers align with the flow of fresh concrete [14,24,30]. This effect is stronger at higher flow velocity [24] and therefore it may be associated to the material plastic viscosity and casting rate. Fiber alignment also increases with the time that fibers are submitted to the flow velocity, or indirectly, with the flow-distance [14,17,30]. Thereby, the influence of flow is inherently related to the casting method and to the geometry of the element itself. Moreover, dependent on the height and width of the formwork, secondary flow may also develop in zones outside the influence of the walls of the formwork [24,30].

Until now, in spite of the recent advances on the link between rheological properties and casting processes of plain concrete [32], the specific influence of the flow on fiber alignment remains unknown. Thereby, further research is required so that the increment of

orientation number due to the flow ($\Delta\eta_{DF}$) can be incorporated in the present framework.

5.4. Influence of the formwork geometry

The effect of the mold sides and a free surface causes fibers to orient parallel to the wall or surface. The quantification of these wall-effects has only been reported in literature by assuming the absence of preferential fiber orientations in the zones out-of-influence of BCs. In this paper an innovative approach was proposed to quantify the increment of orientation number due to wall-effects in the three independent axes and for any η in the bulk of a section. Thereby, similarly to the previous stages of this framework, the orientation number after passing walls of the formwork in any direction i (η_{Fi}) is obtained through an additive process by:

$$\eta_{Fi} = \eta_{Di} + \Delta\eta_{FWi}. \quad (17)$$

Given that no further stages of the production process occur that influence fiber orientation, the latter also coincides with η in the hardened-state:

$$\eta_{\theta i} = \eta_{Fi}. \quad (18)$$

Note that, due to the tendency towards planar fiber orientation of SCC, this material was idealized as having a fictitious horizontal BC equal to a fiber length. Thereby, η under the influence of one side of the formwork (η_i) corresponds to the actual value in the bulk of the cross-section (η_D) and the increment of η only accounts for the vertical sides of the mold.

5.5. Summary

The proposed framework implies a stepwise calculation of several production stages that play major influence on fiber orientation. The steps required to determine $\eta_{\theta i}$ are summarized in Table 3.

According to the sequential procedure shown in Table 3, $\eta_{\theta i}$ can be predicted by:

$$\eta_{\theta i} = \eta_{Mi} + \Delta\eta_{Ci} + \Delta\eta_{Di} + \Delta\eta_{FWi}. \quad (19)$$

Or, alternatively, in its extended form:

$$\eta_{\theta i} = \eta_{Mi} + (\Delta\eta_{CW} \times C_{Di}) + (\Delta\eta_{DVi} + \Delta\eta_{DFi}) + \Delta\eta_{FWi}. \quad (20)$$

Table 3

Summary of the steps required to apply the proposed framework.

1. Fresh-state properties after mixing (η_{Mi})
 - 1.1 Select the type of FRC (Table 1)
2. Casting method ($\Delta\eta_{Ci}$)
 - 2.1. Identify casting direction (φ and β) and determine η_{Co} (Eq. (9))
 - 2.2. Calculate wall-effects induced by the casting element, $\Delta\eta_{CW}$ (Table A3.1)
 - 2.3. Determine C_{Di} (Table 2)
 - 2.4. Obtain $\Delta\eta_{Ci}$ (Eq. (10))
3. Dynamic effects ($\Delta\eta_{Di}$)
 - 3.1. Quantify the influence of external vibration, $\Delta\eta_{Dvi}$
 - 3.2. Quantify the influence of flow, $\Delta\eta_{DFi}$
4. Formwork geometry ($\Delta\eta_{FWi}$)
 - 4.1. Determine wall-effects introduced by the formwork, $\Delta\eta_{FWi}$ (Table A3.1)
5. Final orientation number ($\eta_{\theta i}$) (Eq. (20))

6. Application of the proposed framework

6.1. Experimental data

Among the extensive experimental research that has been done on fiber orientation there is, unfortunately, a significant part of works that do not provide information on the specific production processes applied. Procedures such as direction of casting, characteristics of casting elements or energies of vibration are commonly omitted and, consequently, results of fiber orientation cannot be used to validate the present framework.

In this section, experimental results from three doctoral thesis carried out at Delft University of Technology are taken into account [14,20,34]. Fiber orientation was analyzed through the image analysis technique both on small and large-scale beams made of self-compacting steel fiber reinforced concrete (SCSFRC).

On the investigation carried out by Grünwald [14], fourteen small beams were produced with various types of fibers. Casting was performed at middle-length of the beams using a shovel. The latter had a cross-section 60 mm wide (B_C) and with lateral walls (H_C) of 30 mm (Fig. 12). Casting direction was 45° with respect both to the longitudinal and vertical axes of the beam (φ and β). The shovel was placed in the beginning of casting on the edge of the mold (150 mm height) and when concrete reached the top, it was about 5 cm higher not to have contact between the concrete and the shovel. Results from this work are herein defined as Cases 1–14.

Schumacher [34] analyzed two large beams of reinforced concrete with steel fibers. Each of the beams was sawed at five different cross-sections along the longitudinal axis, thus providing a total of ten independent results (Cases 15–24). Given the small amount of conventional reinforcement, the effect of the latter on fiber orientation was considered negligible. Casting of the beams was performed with a concrete trolley which, once touching one of the lateral sides of formwork, was lifted and rotated. The maximum casting height was the depth of the beam (300 mm). This way, filling was done along with the vertical of the beam (y-axis). Given the geometry of the concrete trolley (large B_C comparatively to L), no preferential orientation due to the pouring element was considered.

The work performed by Markovic [20] embraced the production of six prismatic beams, four of which were made of hybrid SCSFRC. The later combined both macro- and micro-fibers which, for the purpose of measuring fiber orientation, were independently analyzed. This way, ten results are herein considered (Cases 25–34). The same shovel used in the first work [14] was applied to cast the concrete. Nonetheless, the casting method was rather different: concrete was poured in layers with thicknesses (H_C) “couple of times smaller than the fiber length” [14] and the direction of casting coincided with the longitudinal axis of the beam (x-axis). No “free-fall” happened during casting, i.e., the several layers of concrete were placed without dropping height.

Further details of the experimental data are listed in Appendix 4. Note that, in all cases considered, step 3 of the proposed framework is omitted because: a) no external vibration occurred; and b) flow-distance was assumed to be negligible regarding that analyzed cross-sections were

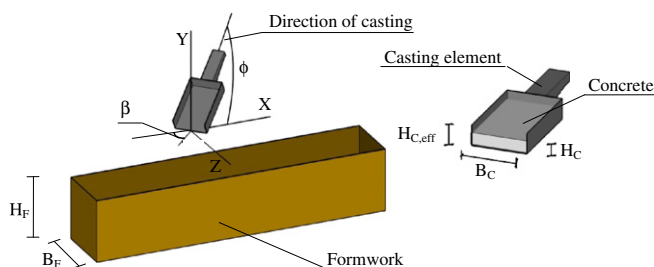


Fig. 12. Schematic representation of the main input parameters.

Table 4

Example of the application of the proposed framework (Case 10).

Main steps	Expression	Application	Result
1	Table 1	Self-compacting concrete	$\eta_{Mx} = \eta_{Mz} = 0.60$; $\eta_{My} = 0.30$
2.1	Eq. (9)	η_{Mx} ; η_{My} ; η_{Mz} ; $\beta = 45^\circ$; $\varphi = 45^\circ$	$\eta_{Co} = 0.474$
2.2	Table A3.1	$B_C = 60.0$ mm; $H_{C,eff} = L = 41.2$ mm; $\eta_0 = \eta_{Co}$	$\Delta\eta_{CW} = 0.286$
2.3	Table 2	β ; φ ; B_C ; $H_{C,eff}$	$C_{Dx} = 0.296$
2.4	Eq. (10)	$\Delta\eta_{CW}$; C_{Dx}	$\Delta\eta_{Cx} = 0.085$
3	Eq. (16)	(Not applicable)	$\Delta\eta_{Dx} = 0.0$
4	Table A3.1	$B_F = 150.0$ mm; $L = 41.2$ mm; $\eta_0 = \eta_{Dx} = 0.685$	$\Delta\eta_{FWx} = 0.049$
5	Eq. (20)	η_{Mx} ; $\Delta\eta_{Cx}$; $\Delta\eta_{Dx}$; $\Delta\eta_{FWx}$	$\eta_{0x} = 0.734$

either closely located (≤ 70 mm) with respect to the pouring zone (Cases 1–14 and 25–34) or had particular conditions (small fiber length with respect to cross-section dimensions) in which flow-distance does not have a significant effect on fiber orientation (Cases 15–24).

6.2. Applying the framework: step-by-step

For clarity, the proposed framework is applied hereafter in detail for Case 10 (Table 4). The main steps defined in Table 3 are followed to calculate the orientation number of the fibers along the longitudinal axis (x-direction). Detailed results of all the other cases considered are listed in Appendix 5.

6.3. Overall results

The comparisons between experimental and predicted orientation numbers in the hardened-state (η_0) for the 34 cases considered are summarized in Fig. 13 (detailed values are presented by Appendix 5). Fig. 13 shows that the proposed framework is able to provide good predictions of the average fiber orientation for a large number of cases, irrespectively of fiber geometry, casting method and formwork geometry. It should be noticed that, in spite of the complexity involved on predicting fiber orientation through such a rational approach, the deviations between predicted and experimental η are not significant. As a matter of fact, the average deviation of the 34 cases was only -3.1% . The maximum absolute deviation was limited to 13.4% and the average absolute deviation of all cases was 5.3% (Appendix 5).

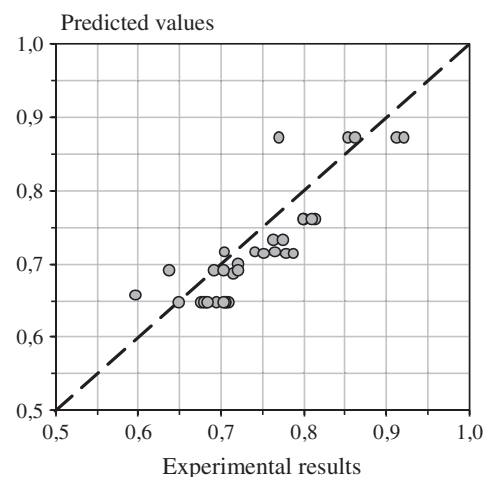


Fig. 13. Overall predictions for the orientation number in the hardened-state (η_0).

7. Conclusions

This paper proposes an ambitious framework aiming to establish a link between fiber orientation with the properties of FRC, the structure to be built and its respective production process. In the first part, the motivations for this investigation were highlighted and the core concepts of this novel framework were advanced. In a second part, two major subjects were analyzed and approached from a theoretical perspective (fiber orientation in 3-D and the wall-effects in anisotropic conditions). Finally, in the last part, the proposed framework was explained in detail and validated with several results from literature.

The need of integrating material characteristics, production processes and the structure itself within a unique framework has never been as recognized as it is in the present. With this paper, a first attempt to combine all these aspects within a comprehensive, straightforward and intuitive approach has been proposed. It has to be noted that, regarding the complexity of the subject, there are some aspects that still require further investigation in order to create a robust and general engineering toolbox to predict fiber orientation. Nonetheless, predictions provided by this framework are very promising: with further experimental validation of some of its assumptions, fiber orientation, probably the most uncertain parameter affecting FRC properties, could be explained within a logical approach.

Acknowledgments

The first author gratefully acknowledges the grant SFRH/BD/36248/2007 provided by *Fundação para a Ciência e a Tecnologia* (FCT) from Portugal.

Appendix 1. Notations

η	= Orientation number [–]
η_M	= η after mixing FRC [–]
η_C	= η after casting FRC into the formwork [–]
η_D	= η after occurrence of dynamic effects [–]
η_F	= η after wall-effects induced by the formwork [–]
η_θ	= η in the hardened-state [–]
η_x	= η along the x-axis [–]
η_y	= η along the y-axis [–]
η_z	= η along the z-axis [–]
η_{xz}	= Sum of η in the x- and z-axes [–]
η_{xyz}	= Sum of η in the x-, y- and z-axes [–]
η_{1D}	= η in the unidirectional case (1-D) [–]
η_{2D}	= η in the planar-random case (2-D) [–]
η_{3D}	= η in the spatial-random case (3-D) [–]
η_0	= η at the zone of the cross-section in bulk [–]
η_{CO}	= η at the zone of the cross-section in bulk after casting [–]
η_{DO}	= η at the zone of the cross-section in bulk after dynamic effects [–]
η_1	= Average η at the zone of the cross-section with one BC [–]
η_2	= Average η at the zone of the cross-section with two orthogonal BCs [–]
L	= Fiber length [mm]
φ	= Vertical angle (starting from the plane xOz) [°]
β	= Horizontal angle (within plane xOz, starting from the x-axis) [°]
A_ξ	= Spherical surface associated to the angle ξ in half-sphere [mm ²]
ξ	= Angle around an independent axis [°]
SL	= Significance level [–]

ξ_{SL}	= Angle around an independent axis providing a significance level α [°]
$\eta_{xz,m}$	= Average sum of η_{xz} [–]
$s(\eta_{xz})$	= Standard deviation of η_{xz} [–]
$\eta_{xyz,m}$	= Average sum of η_{xyz} [–]
$s(\eta_{xyz})$	= Standard deviation of η_{xyz} [–]
$\Delta\eta_W$	= Increment of η due to wall-effects [–]
η_{CO}	= η in bulk of the casting element [–]
B_C	= Width of concrete in the cross-section of the casting element [mm]
H_C	= Height of concrete in the cross-section of the casting element [mm]
$H_{C,eff}$	= Effective H_C [mm]
D_C	= Diameter of concrete in the cross-section of the casting element [mm]
$\Delta\eta_{Ci}$	= Increment of η in direction i due to casting method [–]
$\Delta\eta_{CW}$	= Increment of η due to wall-effects of the casting element [–]
C_{Di}	= Parameter accounting for misalignment between casting direction and direction i of the formwork. [–]
$\Delta\eta_{Di}$	= Increment of η in direction i due to dynamic effects [–]
$\Delta\eta_{DVi}$	= Increment of η in direction i due to external vibration [–]
$\Delta\eta_{DFi}$	= Increment of η in direction i due to flow [–]
$\Delta\eta_{FWi}$	= Increment of η in direction i due to wall-effects of the formwork [–]
h_i	= Distance between fiber gravity point and the horizontal BC [mm]
b_i	= Distance between fiber gravity point and the vertical BC [mm]
A_0	= Area of the cross-section with zero BCs [mm ²]
A_1	= Area of the cross-section with one BC [mm ²]
A_2	= Area of the cross-section with two orthogonal BCs [mm ²]

Appendix 2. Wall-effects under isotropic conditions

The orientation number (η) of a single fiber is the ratio between its projected length on a certain axis and its total length. When all the possible orientations of the fiber are considered, its end-points describe a spherical surface with radius (R) equal to half the fiber length. In isotropic conditions, all the points of the sphere have equal probability of occurrence. Thereby, η can be calculated as the ratio between the projected spherical surface along the considered axis (P_S) and the total spherical surface (A_S):

$$\eta = \frac{P_S}{A_S} \quad (A2.1)$$

A2.1. Orientation number of a fiber with one boundary condition

When fiber rotation capacity is restrained by one boundary condition (BC) its end-points describe a sphere that is cut by two symmetric sphere caps. Consider, for instance, that such BC is horizontal (Fig. A2.1a) and is located at a distance h from the fiber gravity point (Eq. (A2.2)). The vertical angle (φ) and the horizontal angle (α) will be considered in order to define the infinitesimal surface (dA), given by Eq. (A2.3) (Fig. A2.1b):

$$h(\varphi_L) = \frac{L}{2} \times \sin\varphi_L \quad (A2.2)$$

$$dA = (R \times d\varphi) \times (r \times d\alpha). \quad (A2.3)$$

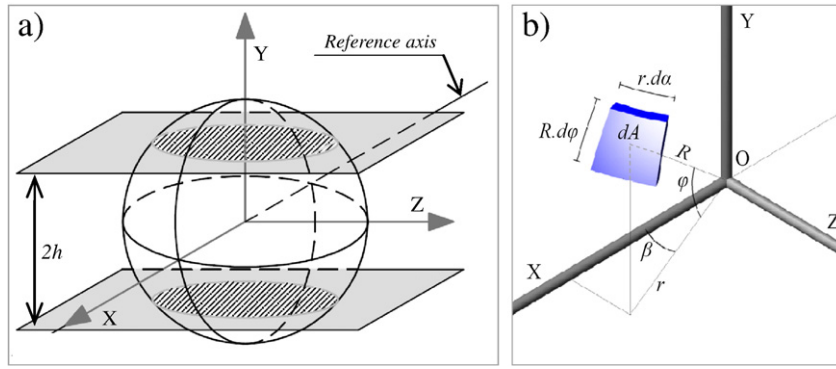


Fig. A2.1. Fiber near one BC: a) overview; and b) identification of main parameters.

In Eq. (A2.2), φ_L is the limit of the vertical angle up to which fiber is not influenced by the BC, whereas r (Eq. (A2.3)) is the horizontal projection of the spherical radius, defined in Eq. (A2.4). Given that no vertical BC exist in this case, α is equal to β (horizontal angle in the plane xOz) and its limit value (α_L) in half-sphere is therefore $\pi/2$.

$$r = R \times \cos\varphi. \quad (\text{A2.4})$$

The available area of half-sphere in the presence of one BC parallel to xOz, $A_{S1}(\varphi_L)$, can then be defined by:

$$A_{S1}(\varphi_L) = \int_{\varphi=-\varphi_L}^{\varphi=\varphi_L} \int_{\alpha=-\frac{\pi}{2}}^{\alpha=\frac{\pi}{2}} dA = 2\pi R^2 \times \sin\varphi_L. \quad (\text{A2.5})$$

The respective projected surface along the x-axis (P_{S1}) is given in Eq. (A2.7) in terms of its infinitesimal surface (dP):

$$dP = dA \times \cos\varphi \times \cos\alpha \quad (\text{A2.6})$$

$$P_{S1}(\varphi_L) = \int_{\varphi=-\varphi_L}^{\varphi=\varphi_L} \int_{\alpha=-\frac{\pi}{2}}^{\alpha=\frac{\pi}{2}} dP = 2R^2 \times (\cos\varphi_L \times \sin\varphi_L + \varphi_L). \quad (\text{A2.7})$$

The orientation number for one BC (η_1) parallel to xOz is then given by:

$$\eta_1(\varphi_L) = \frac{P_{S1}}{A_{S1}} = \frac{1}{\pi} \times \left(\cos\varphi_L + \frac{\varphi_L}{\sin\varphi_L} \right). \quad (\text{A2.8})$$

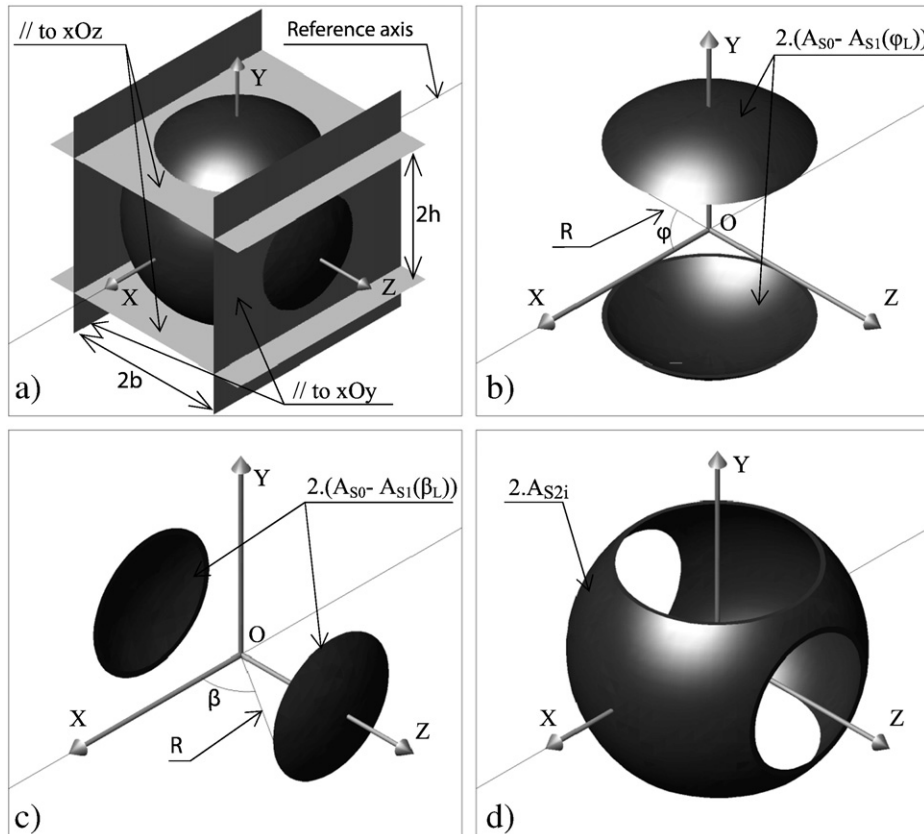


Fig. A2.2. Fiber near a corner with two independent wall-effects.

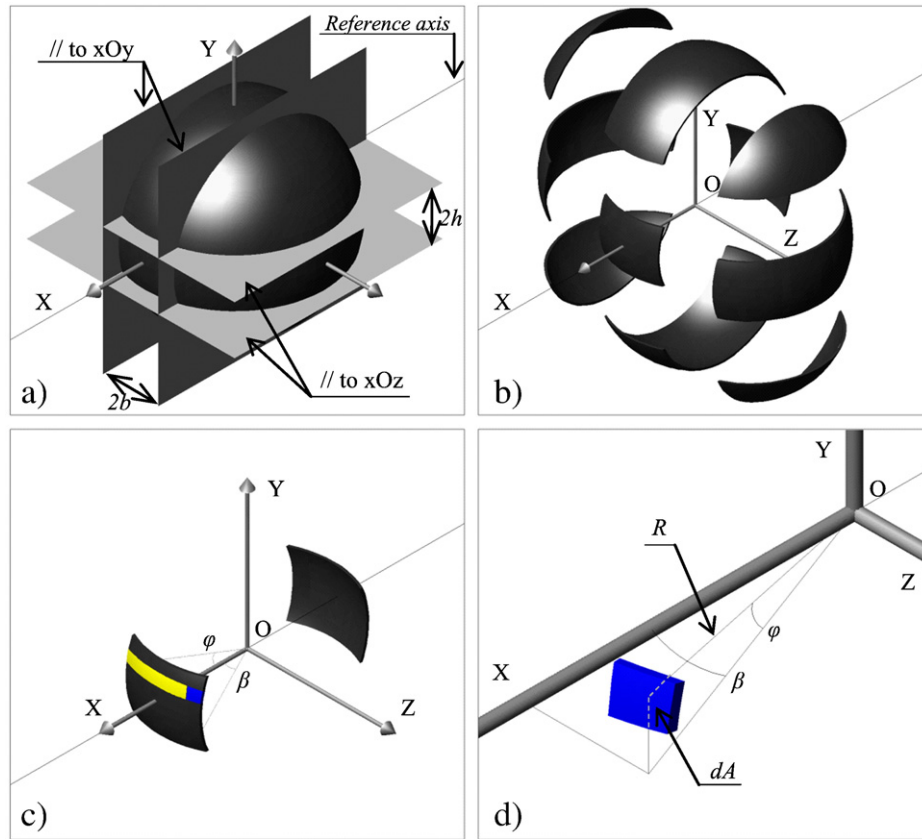


Fig. A2.3. Fiber near a corner with two dependent wall-effects.

Given that the solution of Eq. (A2.8) is a Bernoulli polynomial, the average η_1 along the bandwidth of influence of the wall requires numerical integration, returning:

$$\eta_1 = \int_{\varphi_L=0}^{\varphi_L=\pi} \eta_1(\varphi_L) \times d\varphi_L \approx 0.60. \quad (\text{A2.9})$$

In the absence of any BC, both α_L and φ_L would be equal to $\pi/2$ and, in that case, Eqs. (A2.2)–(A2.9) would provide an average orientation number (η_0) equal to 0.50.

A2.2. Orientation number of a fiber with two boundary conditions

When a fiber is under the influence of two orthogonal BCs its end-points describe a sphere that is cut by two pairs of symmetric sphere caps (Fig. A2.2). The magnitude of the surfaces

extracted by each pair of caps depends on the distance of the gravity point of the fiber (L_{GP}) to each of the walls. This way, two different scenarios may occur: either the pairs of sphere caps are independent between each other ($\beta_L + \varphi_L \geq \pi/2$) or they intersect themselves due to short proximity of L_{GP} to both walls ($\beta_L + \varphi_L < \pi/2$).

A2.2.1. Case 1: independent wall-effects ($\beta_L + \varphi_L \geq \pi/2$)

When the wall-effects of two BCs are independent from each other, the range of possible fiber orientations is defined accordingly with Fig. A2.2. Starting from the total spherical surface (Fig. A2.2a), the pairs of sphere caps referring to the wall parallel to xOz (Fig. A2.2b) and the one parallel to xOy (Fig. A2.2c) have to be extracted in order to obtain the portion of the spherical surface where fiber end-points can be located (Fig. A2.2d).

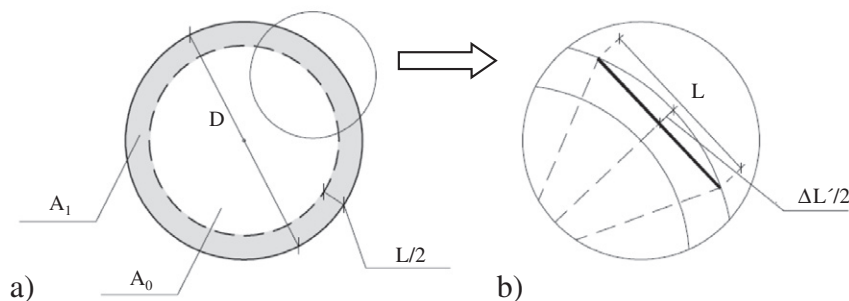


Fig. A3.1. Circular cross-section: a) sub-areas; and b) detail of the “chord-effect”.

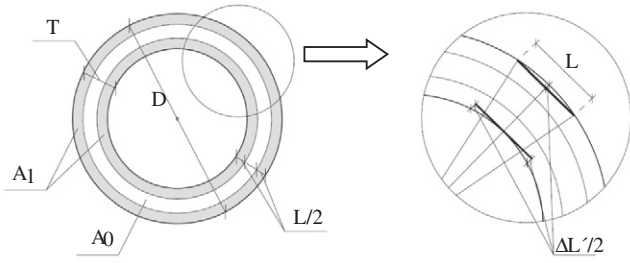


Fig. A3.2. Hollow-circular cross-section: a) sub-areas; and b) balanced "chord-effect".

The half of the total spherical surface (A_{S0}) and its respective projection along the x-axis (P_{S0}) can be obtained by fixing φ_L equal to $\pi/2$ in Eqs. (A2.5) and (A2.7), respectively. $A_{S1}(\varphi_L)$ is the remaining surface of half-sphere after extraction of the sphere-cap parallel to the xOz plane and its respective projection in the x-axis is defined as $P_{S1}(\varphi_L)$. Similarly, $A_{S1}(\beta_L)$ is the remaining surface of half-sphere after extraction of the sphere-cap parallel to the xOy plane and its respective projection in the x-axis is defined as $P_{S1}(\beta_L)$. Note that in this case, α and β are no longer the same values and therefore Eq. (A2.10) has to be considered for the limit angle α_L .

With the previous parameters, the total surface in the presence of two independent wall-effects A_{S2i} (Eq. (A2.11)), the respective projection in the x-axis, P_{S2i} (Eq. (A2.12)) and the respective orientation number, η_{2i} (Eq. (A2.13)) can be obtained:

$$\alpha_L = a \sin\left(\frac{\sin\beta_L}{\cos\varphi}\right) \quad (\text{A2.10})$$

$$A_{S2i}(\varphi_L, \beta_L) = A_{S0} - (A_{S0} - A_{S1}(\varphi_L)) - (A_{S0} - A_{S1}(\beta_L)) = 2\pi R^2(\sin\varphi_L + \sin\beta_L - 1) \quad (\text{A2.11})$$

$$P_{S2i}(\varphi_L, \beta_L) = P_{S0} - (P_{S0} - P_{S1}(\varphi_L)) - (P_{S0} - P_{S1}(\beta_L)) = 2R^2(\cos\varphi_L \cdot \sin\varphi_L + \cos\beta_L \cdot \sin\beta_L + \varphi_L + \beta_L) - \pi R^2 \quad (\text{A2.12})$$

$$\eta_{2i} = \frac{P_{S2i}}{A_{S2i}} = \frac{2 \times (\cos\varphi_L \cdot \sin\varphi_L + \cos\beta_L \cdot \sin\beta_L + \varphi_L + \beta_L) - \pi}{2\pi \times (\sin\varphi_L + \sin\beta_L - 1)} \quad (\text{A2.13})$$

A2.2.2. Case 2: dependent wall-effects ($\beta_L + \varphi_L < \pi/2$)

When the L_{GP} is at short distance to both of the orthogonal BCs, the extracted sphere caps from both walls superpose each other (Fig. A2.3a). Thereby, among the total amount of spherical fragments generated by the intersections with the walls (Fig. A2.3b), there is a reduced available surface where fiber end-points can be located (Fig. A2.3c). To calculate the orientation number of a fiber submitted to these two dependent wall-effects (η_{2d}) the infinitesimal surface dA (Eq. (A2.3)) has to be considered (Fig. A2.3d). Thereby, the available surface in the presence of two dependent wall-effects is given by:

$$A_{S2d} = \int_{\varphi=-\varphi_L}^{\varphi=\varphi_L} \int_{\alpha=-\alpha_L}^{\alpha=\alpha_L} dA = 4R^2 \left[\sin\beta_L \times a \tan(K) - a \tan(\sin\beta_L \times K) + \sin\varphi_L \times a \sin\left(\frac{\sin\beta_L}{\cos\varphi_L}\right) \right] \quad (\text{A2.14})$$

With K being a ratio of the distances between planes parallel to xOz and xOy:

$$K = \frac{\tan\varphi_L}{\sqrt{1 - \left(\frac{\sin\beta_L}{\cos\varphi_L}\right)^2}} \quad (\text{A2.15})$$

And the respective projected surface in the x-axis (P_{S2d}) defined such as:

$$P_{S2d} = \int_{\varphi=-\varphi_L}^{\varphi=\varphi_L} \int_{\alpha=-\alpha_L}^{\alpha=\alpha_L} dP = 4R^2 \times \sin\varphi_L \times \sin\beta_L \quad (\text{A2.16})$$

Consequently, the orientation number of a fiber subjected to two BCs with dependent wall-effects (η_{2d}) is given by:

$$\eta_{2d} = \frac{P_{S2d}}{A_{S2d}} = \frac{\sin\varphi_L \times \sin\beta_L}{\sin\beta_L \times a \tan(K) - a \tan(\sin\beta_L \times K) + \sin\varphi_L \times a \sin\left(\frac{\sin\beta_L}{\cos\varphi_L}\right)} \quad (\text{A2.17})$$

A2.2.3. Average orientation number of a fiber with 2 BCs

Once the orientation number of a fiber with 2 BCs is defined for the two possible scenarios previously defined, it can then be integrated along the bandwidth of influence of both walls to obtain the average orientation number (η_2):

$$\eta_2 = \int_{\varphi_L+\beta_L=0}^{\varphi_L+\beta_L=\frac{\pi}{2}} \eta_{2d} \times d\varphi_L \times d\beta_L + \int_{\varphi_L+\beta_L=\frac{\pi}{2}}^{\varphi_L+\beta_L=\pi} \eta_{2i} \times d\varphi_L \times d\beta_L \approx 0.84 \quad (\text{A2.18})$$

Appendix 3. Generalized wall-effects for common cross-section geometries

The influence of the cross-section geometry on the average orientation of fibers can be quantified through the averaging procedure depicted in Fig. 8. This way, the orientation number is simply defined by:

$$\eta = \frac{A_0 \times \eta_0 + A_1 \times \eta_1 + A_2 \times \eta_2}{A_0 + A_1 + A_2} \quad (\text{A3.1})$$

Alternatively, η can also be obtained by adding to the average orientation in bulk (η_0) the respective increment due to the wall-effects for the entire cross-section, $\Delta\eta_W$ (Eq. (A3.2)). The latter is defined in Eq. (A3.3) in terms of the average increments of the orientation number due to one BC ($\Delta\eta_1$) and two BCs ($\Delta\eta_2$). According to Eqs. (13) and (14), $\Delta\eta_1$ and $\Delta\eta_2$ can be quantified uniquely in terms of η_0 , such as shown in Eqs. (A3.4) and (A3.5), respectively.

$$\eta = \eta_0 + \Delta\eta_W \quad (\text{A3.2})$$

$$\Delta\eta_W = \frac{A_1 \times \Delta\eta_1 + A_2 \times \Delta\eta_2}{A_0 + A_1 + A_2} \quad (\geq 0) \quad (\text{A3.3})$$

$$\Delta\eta_1 = \eta_1 - \eta_0 \quad (\geq 0) \quad (\text{A3.4})$$

$$\Delta\eta_2 = \eta_2 - \eta_0 \quad (\geq 0) \quad (\text{A3.5})$$

Regarding Eqs. (A3.1)–(A3.5), the quantification of the wall-effects can be generalized for any η_0 through simple and straightforward expressions for the most common cross-section geometries. However, in the case of SCC, the wall-effects introduced by horizontal BCs may be negligible given the intrinsic tendency of fibers to align in horizontal planes. Thereby, $\Delta\eta_W$ of SCC depends on whether the cross-section is contained or not in the vertical plane. When the latter occurs, the assumption previously advanced for the fresh-state properties of SCC implies a distance between horizontal boundaries (H) equal to the fiber length (L). Consequently, η_0 becomes equal to η_1 and the values obtained from Eqs. (A3.4)–(A3.5) provide simpler expressions.

A3.1. Rectangular cross-section

According to Fig. 8, the sub-areas A_0 , A_1 and A_2 of a rectangular cross-section are defined uniquely in terms of its width (B), height (H) and fiber length (L):

$$A_0 = (B-L) \times (H-L) \quad (\geq 0) \quad (\text{A3.6})$$

$$A_1 = (B-L) \times L + (H-L) \times L \quad (\geq 0) \quad (\text{A3.7})$$

$$A_2 = L^2 \quad (\geq 0). \quad (\text{A3.8})$$

Introducing Eqs. (A3.4)–(A3.8) in Eq. (A3.3), $\Delta\eta_w$ can then be obtained for CC:

$$\Delta\eta_w = \frac{L^2}{B \times H} \left[\frac{B+H}{L} (0.465 - 0.730\eta_0) + 0.533\eta_0 - 0.127 \right]. \quad (\text{A3.9})$$

In case of SCC, Eq. (A3.9) applies whenever the tendency of fibers towards horizontal orientations does not influence the wall-effects (cross-sections in horizontal plane). On the other hand, for cross-sections in the vertical plane, a simplified expression is obtained given that an intrinsic horizontal BC is being assumed for SCC in bulk. Hence, only the vertical walls play major influence (Eq. (A3.10)). This will occur for any geometry considered for the cross-section.

$$\Delta\eta_w = \frac{L}{B} \times (0.677 - 0.73 \times \eta_0). \quad (\text{A3.10})$$

A3.2. Circular cross-section

Cross-sections with circular geometry can be subdivided in two zones, with zero and one BCs (A_0 and A_1 , respectively), as shown in Fig. A3.1a. These sub-areas are defined by Eqs. (A3.11) and (A3.12), respectively:

$$A_0 = \frac{\pi}{4} \times (D-L^*)^2 \quad (\geq 0). \quad (\text{A3.11})$$

$$A_1 = \frac{\pi}{4} \times L^* (2 \times D - L^*) \quad (\geq 0). \quad (\text{A3.12})$$

Adding Eqs. (A3.3)–(A3.5) and Eqs. (A3.11) and (A3.12), $\Delta\eta_w$ can be simply defined by:

$$\Delta\eta_w = \frac{L^* \times (2D - L^*)}{D^2} \times (0.465 - 0.730\eta_0). \quad (\text{A3.13})$$

However, in case of vertical cross-sections with SCC, $\Delta\eta_w$ is obtained by:

$$\Delta\eta_w = \frac{L^* \times (2D - L^*)}{D^2} \times (0.677 - 0.730\eta_0). \quad (\text{A3.14})$$

Due to the curved shape of the walls in circular cross-sections, the gravity-point of the fiber no longer reaches the BC because fiber end-points are restrained in their rotation ability. This phenomenon is herein defined as the “chord-effect” (Fig. A3.1b) and, for practical purposes, it implies an increment of the bandwidth of influence of the BC (ΔL) which is then provided in terms of a corrected fiber length (L^*):

$$L^* = L + \Delta L. \quad (\text{A3.15})$$

According to its mathematical definition (A3.16), the chord of an angle θ is the length of the chord between two points on a unit circle separated by that angle. Regarding Fig. A3.1b, it can be seen that this chord corresponds to the fiber length (A3.17) and, consequently, the angle to the center (θ) can be obtained (Eq. (A3.18)).

$$\text{chord}(\theta) = 2 \times \sin\left(\frac{\theta}{2}\right) \quad (\text{A3.16})$$

$$L = \text{chord}(\theta) \times \frac{D}{2} \quad (\text{A3.17})$$

$$\theta = 2 \times \sin\left(\frac{L}{D}\right). \quad (\text{A3.18})$$

The maximum distance between the fiber and the curved wall ($\Delta L'$) is, by definition, equal to:

$$\Delta L' = \frac{D}{2} \times \left[1 - \cos\left(\frac{\theta}{2}\right) \right]. \quad (\text{A3.19})$$

Regarding Eqs. (A3.18) and (A3.19) and the fact that $\Delta L'$ has to be considered twice for the whole cross-section, ΔL thus returns:

$$\Delta L = D \times \left[1 - \cos\left(\sin\left(\frac{L}{D}\right)\right) \right]. \quad (\text{A3.20})$$

It should be noted that when $D \gg L$, then $\Delta L^* \approx 0$ and, consequently, the chord-effect is negligible. On the other hand, if D is not much larger than L , neglecting Eq. (A3.20) underestimates the overall orientation number. For instance, for a cross-section with 150 mm diameter and fibers with 60 mm length (Fig. A3.1), the value of $\Delta\eta_w$ without considering the chord-effect is approximately 13% lower.

A3.3. Hollow-circular cross-section

This type of cross-section geometries can be subdivided in two zones, with zero and one BCs (A_0 and A_1 , respectively), as shown in Fig. A3.2a. Both A_1 (Eq. (A3.21)) and the sum of A_1 with A_0 (Eq. (A3.22)) can be defined in terms of the external and internal diameters (D_e and D_i , respectively):

$$A_1 = \frac{\pi}{4} \times L \times (D_i + D_e) \quad (\geq 0) \quad (\text{A3.21})$$

$$A_1 + A_0 = \frac{\pi}{4} \times (D_e^2 - D_i^2) \quad (\geq 0). \quad (A3.22)$$

Adding Eqs. (A3.3)–(A3.5) and Eqs. (A3.21) and (A3.22) and considering the thickness of the cross-section (T) as the difference between D_e and D_i , $\Delta\eta_w$ can then be defined by:

$$\Delta\eta_w = \frac{L}{T} \times (0.465 - 0.730\eta_0). \quad (A3.23)$$

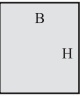
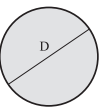
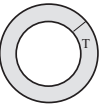
However, in case of vertical cross-sections with SCC, $\Delta\eta_w$ is obtained by:

$$\Delta\eta_w = \frac{L^* \times (2D - L^*)}{D^2} \times (0.677 - 0.730\eta_0). \quad (A3.24)$$

In contrast with circular cross-sections, the chord-effect was not introduced in Eqs. (A3.23) and (A3.24). This occurs because, as shown in Fig. A3.2b, the increment of bandwidth introduced by the external wall is balanced by an approximately similar reduction inferred by the internal wall.

A3.4. Summary

Increments of η for any η_0 and common cross-section geometries.

Cross-section		Type of concrete	Increment of η due to wall-effects ($\Delta\eta_w$)
Geometry	Position		
 B = Width H = Height L = Fiber length	Vertical	SCC	$\Delta\eta_w = \frac{L}{B} \times (0.677 - 0.730 \times \eta_0)$
	Horizontal or inclined	CC	$\Delta\eta_w = \frac{L^*}{B \times H} \left[\frac{B+H}{L} (0.465 - 0.730\eta_0) \right]$
		SCC	$+0.533\eta_0 - 0.127]$
		CC	
 D = Diameter L = Fiber length	Vertical	SCC	$\Delta\eta_w = \frac{L^* \times (2D - L^*)}{D^2} (0.677 - 0.730\eta_0)$
	Horizontal or inclined	CC	$\Delta\eta_w = \frac{L^* \times (2D - L^*)}{D^2} (0.465 - 0.730\eta_0)$
		SCC	$L^* = L + \Delta L$ $\Delta L = D \times \left[1 - \cos \left(a \sin \left(\frac{L}{D} \right) \right) \right]$
		CC	
 T = Thickness L = Fiber length	Vertical	SCC	$\Delta\eta_w = \frac{L}{T} (0.677 - 0.730\eta_0)$
	Horizontal or inclined	CC	$\Delta\eta_w = \frac{L}{T} (0.465 - 0.730\eta_0)$
		SCC	
		CC	

Note: When calculating $\Delta\eta_{cw}$, if concrete is poured with free top-surface:

$$H = H_{c,eff} = \begin{cases} \min\{2 \times H_c, L\} & \text{if SCC} \\ 2 \times H_c & \text{if CC} \end{cases}$$

Appendix 4. Input data for experimental validation

Experimental data used for validation of the proposed framework.

Ref.	Case	Fiber		Casting method				Formwork	
		Characteristics		Direction		Geometry		Geometry	
		L [mm]	d [mm]	φ [°]	β [°]	B _C [mm]	H _{C,eff} [mm]	B _F [mm]	H _F [mm]
[14]	1	30.5	0.39	45	45	60	30.5	150	150
	2	20.2	0.31				20.2		
	3	41.2	0.64				41.2		
	4	28.8	0.62				28.8		
	5	61.1	0.71				60.0		
	6	30.5	0.39				30.5		
	7	30.5	0.39				30.5		
	8	61.1	0.71				60.0		
	9	28.8	0.62				28.8		
	10	41.2	0.64				41.2		
	11	61.1	0.71				60.0		
	12	28.8	0.62				28.8		
	13	61.1	0.71				60.0		
	14	13.0	0.16				13.0		
[34]	15	30	0.375	90	*	**	**	150	300
	16								
	17								
	18								
	19								
	20								
	21								
	22								
	23								
	24								
[20]	25	6	0.16	≈0	0	60	6	150	150
	26	13	0.20				13		
	27								
	28								
	29								
	30	60	0.70				60		
	31								
	32								
	33								
	34								

* Indifferent.

** Very large number (Influence of the casting element is assumed to be negligible).

Appendix 5. Results from experimental validation

Detailed results from the experimental validation.

Case	η_{Mx}	$\Delta\eta_{Cx}$			$\Delta\eta_{Dx}$		$\Delta\eta_{FWx}$	η_{Bx}		Absolute deviation		
		η_{Co}	$\Delta\eta_{CW}$	C_{Dx}	$\Delta\eta_{DVx}$	$\Delta\eta_{DFx}$		Predicted	Exp.			
1	0.600	0.474	0.243	0.331	0.0	0.0	0.037	0.717	0.741	3.2%		
2			0.201	0.374			0.025	0.700	0.721	2.9%		
3			0.286	0.296			0.049	0.734	0.763	3.9%		
4			0.236	0.338			0.035	0.714	0.779	8.3%		
5			0.372	0.250			0.070	0.763	0.813	6.2%		
6			0.243	0.331			0.037	0.717	0.765	6.3%		
7			0.243	0.331			0.037	0.717	0.704	1.9%		
8			0.372	0.250			0.070	0.763	0.800	4.7%		
9			0.236	0.338			0.035	0.714	0.751	4.9%		
10			0.286	0.296			0.049	0.734	0.774	5.2%		
11			0.372	0.250			0.070	0.763	0.799	4.5%		
12			0.236	0.338			0.035	0.714	0.787	9.2%		
13			0.372	0.250			0.070	0.763	0.810	5.8%		
14			0.172	0.411			0.016	0.687	0.715	3.9%		
15	0.600	0.300	0.246	0.000	0.0	0.00	0.048	0.648	0.682	5.0%		
16								0.709	8.6%			
17								0.705	8.1%			
18								0.676	4.2%			
19								0.694	6.7%			
20								0.706	8.2%			
21								0.679	4.6%			
22								0.684	5.3%			
23								0.703	7.9%			
24								0.649	0.2%			
25	0.600	0.600	0.049	1.000	0.0	0.0	0.008	0.657	0.596	10.3%		
26								0.075	0.016	0.691	0.637	8.5%
27								0.691	0.691	0.1%		
28								0.703	1.6%			
29								0.721	4.1%			
30			0.251						0.022	0.873	0.912	4.3%
31											0.921	5.2%
32											0.853	2.3%
33											0.862	1.3%
34											0.770	13.4%
Average deviation									5.3%			

References

- [1] M. di Prisco, G. Plizari, Precast SFRC element: from material properties to structural applications, Proceedings from the 6th RILEM Symposium on FRC. Varenna, Italy, 2004, pp. 81–100.
- [2] A. Aguado, Tendencies of fiber reinforced concrete in underground constructions, Cem. Hormig. 74 (903) (2007) 44–55 (in Spanish).
- [3] A. de la Fuente, J. Armengou, Structural applications of FRC: sewer pipes, panels and soil reinforced walls, Proceedings from Conference on Structural Applications with Fiber Reinforced Concrete (www.bmbupc.org). Barcelona, Spain, 2007, pp. 97–164.
- [4] A. Domingo, C. Lázaro, P. Serna, Use of steel fiber reinforced concrete in thin shell structures: evaluation of fiber performance through testing of shell specimens, Computational Methods for Shell and Spatial Structures (IASS-IACM). Athens, Greece, 2000.
- [5] J.P. Romualdi, J.A. Mandel, Tensile strength of concrete affected by uniformly distributed and closely spaced short lengths of wire reinforcement, ACI J. 61 (6) (1964) 27–37.
- [6] C.V.S. Kameswara Rao, Effectiveness of random fibres in composites, Cem. Concr. Res. 9 (1979) 685–693.
- [7] H. Krenchel, Fibre spacing and specific fibre surface, in: A. Neville (Ed.), Fibre Reinforced Cement and Concrete, The Construction Press, UK, 1975, pp. 69–79.
- [8] P. Soroushian, C. Lee, Distribution and orientation of fibers in steel fiber reinforced concrete, ACI Mater. J. 87 (5) (1990) 433–439.
- [9] C.W. Hoy, Mixing and mix proportioning of fibre reinforced concrete. PhD Thesis. University of Paisley, Scotland, 1998.
- [10] P. Stroeven, Steel fibre reinforcement at boundaries in concrete elements, Proceedings of the 3rd International Workshop on High Performance Fiber Reinforced Cement Composites (HPFRCC3), Mainz, Germany, 1999, pp. 413–421.
- [11] A. Kooiman, Modelling Steel Fibre Reinforced Concrete for Structural Design. PhD Thesis. Delft University of Technology, The Netherlands, 2000.
- [12] A. van Gysel, Study of the pullout behavior of steel fibers embedded in cement-bonded matrix with application on fiber reinforced concrete in bending. PhD Thesis. University of Ghent, Belgium, 2000 (in Dutch).
- [13] D. Dupont, L. Vandewalle, Distribution of steel fibres in rectangular sections, Cem. Concr. Compos. 27 (2005) 391–398.
- [14] S. Grünewald, Performance-based design of self-compacting fibre reinforced concrete. PhD Thesis. Delft University of Technology, The Netherlands, 2004.
- [15] L. Ferrara, Y.D. Park, Shah, A method for mix-design of fiber-reinforced self-compacting concrete, Cem. Concr. Res. 37 (6) (2007) 957–971.
- [16] P. Stähli, J.G.M. van Mier, Manufacturing, fibre anisotropy and fracture of hybrid fibre concrete, Eng. Fract. Mech. 74 (2007) 223–242.
- [17] L. Ferrara, Y.D. Park, S.P. Shah, Correlation among fresh state behavior, fiber dispersion and toughness properties of SFRCs, J. Mater. Civ. Eng. 20 (7) (2008) 493–501.
- [18] L. Martinie, P. Rossi, N. Roussel, Rheology fiber reinforced cementitious materials: classification and prediction, Cem. Concr. Res. 40 (2) (2010) 226–234.
- [19] H. Toujanji, Z. Bayasi, Effects of manufacturing techniques on the flexural behavior of steel fiber-reinforced concrete, Cem. Concr. Res. 28 (1) (1998) 115–124.
- [20] I. Markovic, High-Performance Hybrid-Fibre Concrete: Development and Utilisation. PhD Thesis. Delft University of Technology, The Netherlands, 2006.
- [21] M.C. Torrijos, J.M. Tobes, B.E. Barragán, R.L. Zerbino, Orientation and distribution of steel fibres in self-compacting concrete, Proceedings from the 7th RILEM Symposium on FRC. Chennai, India, 2008, pp. 729–738.
- [22] J. Edington, D.J. Hannant, Steel fibre reinforced concrete. The effect on fibre orientation of compaction by vibration, Mater. Struct. 5 (25) (1972) 41–44.
- [23] R. Gettu, D.R. Gardner, H. Saldívar, B.E. Barragán, Study of the distribution and orientation of fibers in SFRC specimens, J. Mater. Struct. 38 (1) (2005) 31–37.
- [24] L. Lappa, High strength fibre reinforced concrete: static and fatigue behavior in bending. PhD Thesis. Delft University of Technology, The Netherlands, 2007.
- [25] F. Laranjeira, Design-oriented constitutive model for steel fiber reinforced concrete. PhD Thesis. Universitat Politècnica de Catalunya, Spain, 2010.
- [26] J. Walraven, Fibre reinforced concrete: a material in development, Proceedings from Conference on Structural Applications with Fiber Reinforced Concrete (www.bmbupc.org). Barcelona, Spain, 2007, pp. 199–213.
- [27] C. Molins, J. Martinez, N. Arnáiz, Distribution of steel fibers in prismatic concrete samples, CD-ROM from the 4th International Structural Concrete Congress (ACHE). Valencia, Spain, 2008 (in Spanish).
- [28] N. Ozyurt, T.O. Mason, S.P. Shah, Correlation of fiber dispersion, rheology and mechanical performance of FRCs, Cem. Concr. Compos. 29 (2007) 70–79.
- [29] Rilem Technical Committee, Final report of RILEM TC 188-CSC casting of self compacting concrete, Mater. Struct. 39 (2006) 937–954.

- [30] P. Stähli, R. Custer, J.G.M. van Mier, On flow properties, fibre distribution, fibre orientation and flexural behaviour of FRC, *Mater. Struct.* 41 (2008) 189–196.
- [31] D. Dozio, SFRC Structures: Identification of the uniaxial tension characteristic constitutive law, PhD Thesis, Politecnico de Milano, Italy, 2008.
- [32] N. Roussel, Rheology of fresh concrete: from measurements to predictions of casting processes, *Mater. Struct.* 40 (2007) 1001–1012.
- [33] P.J. Robins, S.A. Austin, P.A. Jones, Spatial distribution of steel fibres in sprayed and cast concrete, *Mag. Concr. Res.* 55 (3) (2003) 225–235.
- [34] P. Schumacher, Rotation Capacity of Self-Compacting Steel Fiber Reinforced Concrete, PhD Thesis, Delft University of Technology, The Netherlands, 2006.
- [35] L. Martinie, N. Roussel, Fiber-reinforced cementitious materials: from intrinsic properties to fiber alignment, in: Khayat, Feys (Eds.), *Design, Production and Placement of Self-Consolidating Concrete*, Rilem Bookseries 1, ISBN: 978-90-481-9663-0, 2010, pp. 407–415.